

# Biomechanical Aspects of Compliant Airways due to Mechanical Ventilation

Kittisak Koombua<sup>\*</sup>, Ramana M. Pidaparti<sup>\*,†,‡</sup>, P. Worth Longest<sup>\*,‡</sup>  
Kevin R. Ward<sup>‡,§</sup>

**Abstract:** Without proper knowledge of mechanical ventilation effects, physicians can aggravate an existing lung injury. A better understanding of the interaction between airflow and airway tissue during mechanical ventilation will be helpful to physicians so that they can provide appropriate ventilator parameters for intubated patients. In this study, a computational model incorporating the interactions between airflow and airway walls was developed to investigate the effects of airway tissue flexibility on airway pressure and stress. Two flow rates, 30 and 60 l/min, from mechanical ventilation were considered. The transient waveform was active inhalation with a constant flow rate and passive exhalation. Results showed that airway tissue flexibility decreased airway pressure at bifurcation sites by approximately 25.06% and 16.91% for 30 and 60 l/min, respectively, and increased wall shear stress (WSS) by approximately 74.00% and 174.91% for 30 and 60 l/min, respectively. The results from the present study suggested that it is very important to consider the interaction between airflow and airway walls when computational models are developed. Results of this study help to better quantify how the airflow rate used in mechanical ventilation, in conjunction with airway tissue flexibility, affects airway pressure and stresses.

## 1 Introduction

Mechanical ventilation is a method that partially or fully assists patients whose respiratory system fails to achieve a gas exchange function due to acute lung injury (ALI), acute respiratory distress syndrome (ARDS), airway disease, pulmonary vascular disease, or parenchymal lung disease (1). It is often considered more of an art than a science since physicians must balance between gas exchange rate and tidal volume to prevent ventilator-associated lung injury (VALI). VALI may contribute to multiple organ dysfunction syndrome (MODS) from volutrauma, atelectrauma or bio-trauma mechanisms (2). Many techniques have been suggested to prevent VALI by using positive end-expiratory pressure (PEEP) and lowering the tidal volume and airway pressure (1); however, there are some drawbacks. Lowering the tidal volume can cause hypercapnia, decrease in aerated lung volume, and increase in shunting and worsening oxygenation (3). In addition, PEEP can cause transient oxygen desaturation, hypotension, barotrauma, arrhythmia, and bacterial translocation (4).

Understanding the interactions between airflow and airway walls in the human respiratory system is the first step for understanding mechanisms during the mechanical ventilation process. Many researchers have developed computational models to investigate the effects of airway diseases, e.g., tumors (5, 6), asthma (7), stenosis (8), COPD (9, 10), and airway geometry, e.g., carinal shape (11) and cartilage rings (12), on airflow and particle deposition in the respiratory tract. However, these models were developed without considering the effects of airway wall motion on the flow field. In other words, the airway walls were assumed to be rigid and could not be deformed or distended by

<sup>\*</sup> Department of Mechanical Engineering, Virginia Commonwealth University, Richmond, VA 23284

<sup>†</sup> Corresponding author. Department of Mechanical Engineering, Virginia Commonwealth University, 401 W. Main Street, Room E3255, Richmond, VA 23284. E-mail: rmpidaparti@vcu.edu

<sup>‡</sup> Reanimation Engineering Shock Center, Virginia Commonwealth University, Richmond, VA 23298

<sup>§</sup> Department of Emergency Medicine, Virginia Commonwealth University

fluid force from the airflow. Human airways are, in fact, soft tissue and can be distended by airflow during mechanical ventilation (1).

In this study, a computational model incorporating the interactions between airflow and airway walls, i.e., a flexible wall model, was developed to investigate the effects of airflow rate during mechanical ventilation on airway pressure, wall shear stress (WSS), and airway stress in the human respiratory tract. The results from the flexible wall model were also compared with those from a rigid wall approximation to evaluate the effect of tissue flexibility on airway pressure and WSS during mechanical ventilation.

## 2 Materials and Methods

The transient interactions between airflow and airway walls during mechanical ventilation were investigated by solving two coupled sets of governing equations with associated boundary conditions.

### 2.1 Airflow equations

The governing equations for transient airflow are Navier-Stokes equations on a moving mesh with the assumption of incompressible flow. These equations govern the principles of mass and momentum conservation and are described below using Einstein's repeated index convention (13).

Conservation of mass

$$\frac{\rho_g}{\sqrt{g}} \frac{\partial}{\partial t} (\sqrt{g}) + \rho_g \frac{\partial}{\partial x_j} \left( u_j - \frac{\partial \tilde{x}_j}{\partial t} \right) = 0 \quad (1)$$

Conservation of momentum

$$\begin{aligned} \frac{\rho_g}{\sqrt{g}} \frac{\partial}{\partial t} (\sqrt{g} u_i) + \rho_g \frac{\partial}{\partial x_j} \left[ \left( u_j - \frac{\partial \tilde{x}_j}{\partial t} \right) u_i \right] \\ = - \frac{\partial p}{\partial x_i} + \mu \frac{\partial^2 u_i}{\partial x_j^2} \end{aligned} \quad (2)$$

In these equations,  $\tilde{x}_i$  represents the moving mesh location,  $\sqrt{g}$  is the metric tensor determinate of the transformation, i.e., the local computational control-volume size,  $\rho_g$  is fluid density,  $p$  is fluid pressure,  $\mu$  is fluid viscosity, and  $u$  is fluid velocity.

### 2.2 Airway wall equations

The governing relations for movement of the airway walls during mechanical ventilation are the time-dependent structural equations and are described below using Einstein's repeated index convention (14)

The equation of motion

$$\frac{\partial \sigma_{ij}}{\partial x_j} + F_i = \rho \frac{\partial^2 u_i}{\partial t^2} \quad (3)$$

and constitutive relations

$$\sigma_{ij} = C_{ijkl} \varepsilon_{kl} \quad (4)$$

In the equation above,  $\sigma$  is the stress in each direction,  $F$  is the body force,  $\rho$  is wall density, and  $u$  is the displacement,  $C$  is the elasticity tensor, and  $\varepsilon$  is the strain in each direction.

### 2.3 Computational method

The effect of fluid pressure on a structure is significant, especially if the structure is flexible, such as human airways. The numerical solutions of the interaction between airflow and airway walls during mechanical ventilation were implemented using two software packages, ANSYS and ANSYS CFX. ANSYS is general-purpose finite element (FE) software for structural modeling and ANSYS CFX is general-purpose computational fluid dynamics (CFD) software for modeling fluid flows. The fluid-structure interaction (FSI) algorithm (15) procedures begin by solving the flow equations to obtain fluid pressure. Structural equations are then solved for the displacement using the fluid pressure as an external force. The flow equations are solved again to obtain the fluid pressure after the structural displacement changes the fluid boundaries. This loop continues until both fluid pressure and structural displacement converge for each time period (see Figure 1).

### 2.4 Airway geometry

This study focused mainly on airway generations 3 to 5 for two reasons. First, these airway generations have less cartilage plates and no rings when compared to the proximal generations; therefore

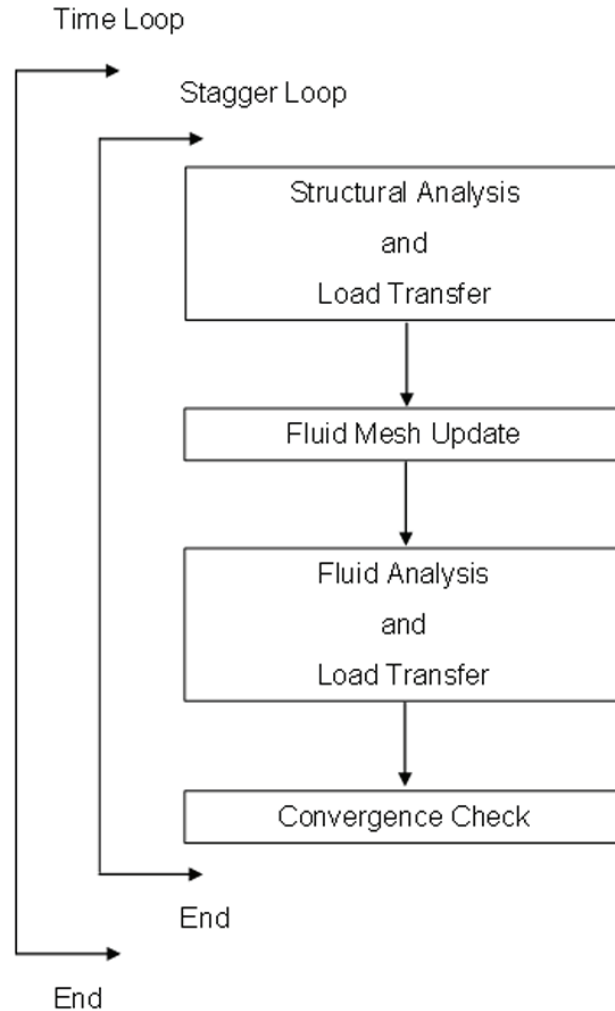


Figure 1: A diagram of the fluid-structure interaction (FSI) algorithm.

the airway walls were assumed to be smooth (16). Second, diameters of these airways do not change as a function of lung volume but their diameters depend on a transmural pressure across the airway walls (1). The geometric dimensions of airway generations 3 to 5 used in this study were based on the ICRP (17) tracheobronchial geometry and airway thickness for each generation was based on measurement by Habib et al. (18) (see Figure 2). The branching angle of the bifurcation was  $70^\circ$  based on the morphological data of Horsfield & Cumming (19). The corresponding geometric diameter, length, and thickness of the bifurcation are tabulated in Table 1. The surface geometry of the model was constructed based on the

physiologically realistic bifurcation (PRB) model suggested by Heistracher & Hofmann (20). This double bifurcation geometry was previously implemented in the study of Longest & Vinchurkar (21), which evaluated the effects of transitional and turbulent flow on particle deposition for a rigid wall assumption.

### 2.5 Computational models and boundary conditions

The computational domains of the bifurcation were created in ANSYS and ANSYS CFX. Due to symmetry, only one half of the domains were constructed. The solid domain was the airway walls with a finite thickness and the fluid do-

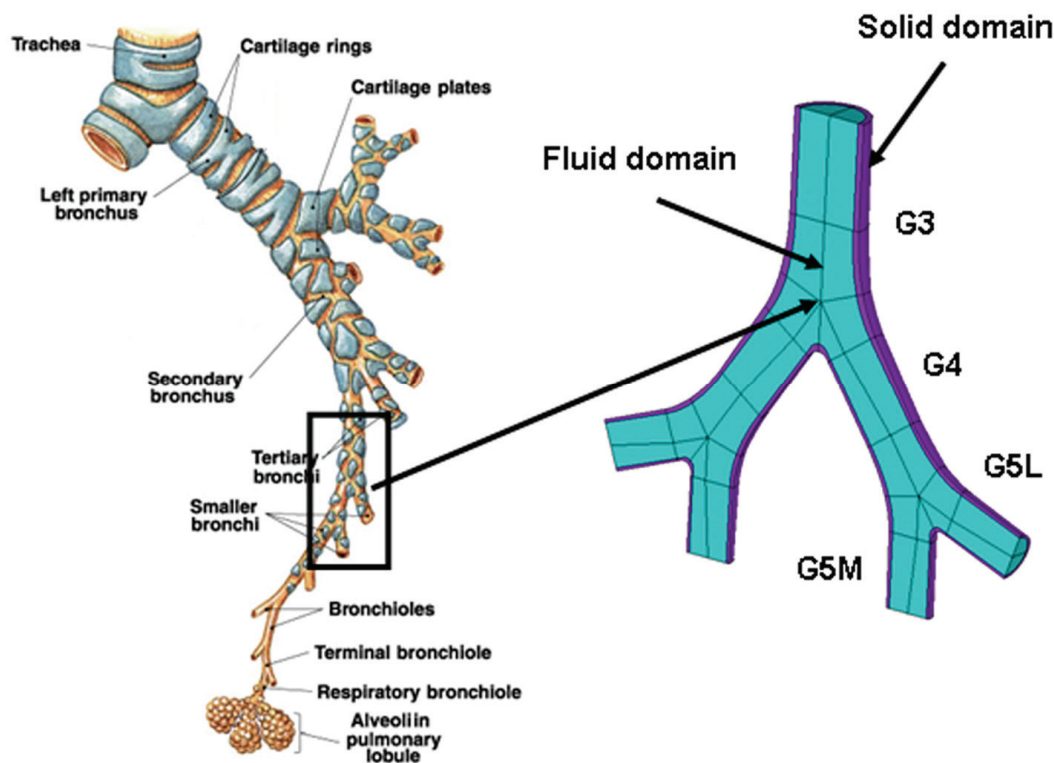


Figure 2: Geometric representations of the airway bifurcation generations 3 to 5 based on ICRP (1994) tracheobronchial geometry and wall thickness measurements by Habib et al. (1994). These bifurcations were used as a computational domain for this study.

Table 1: Parameters for airway generations 3 to 5 based on ICRP (1994) tracheobronchial geometry and wall thickness measurements by Habib et al. (1994)

Generation	Diameter (cm)	Length (cm)	Thickness (cm)
3	0.56	1.1	0.053
4	0.45	0.92	0.041
5	0.36	0.77	0.024

main was the internal volume of air in the bifurcation. Solid elements were used to represent the solid domain and fluid elements were used to represent the fluid domain. A structural hexahedral mesh was employed to provide a high quality flow field solution, as suggested by Longest & Vinchurkar (22) and Vinchurkar & Longest (23). A mesh-independence study was performed on the solid and fluid domains to confirm that a sufficiently fine mesh had been used to represent both solid and fluid domains. The mesh-independence

study began with a mesh discretization and obtaining a solution for one inhaling/exhaling cycle. Then the finer elements were used to represent both solid and fluid domains. The results from the finer-element model were then compared with those from the first model. If the results are nearly similar, then the first mesh results are probably sufficient for that particular geometry, loading and constraints. If the results differ by a large amount, the process was repeated with the finer elements. Maximum pressure and velocity

were used as convergence criteria for the fluid domain and maximum displacement and von Mises stress were used as convergence criteria for the solid domain. A converged model was obtained when changes in those solutions were less than 5%. Having performed the mesh-independence study, the airflow velocity from the finite element model in a center of airway generation 4 was then compared to the experiment by Zhao & Lieber (24). Good agreement was obtained between the simulation and experimental results (22).

The airway wall was assumed to be of a homogeneous and isotropic material with a density of  $1365.6 \text{ kg/m}^3$  (25), a Young's modulus of elasticity in longitudinal direction of  $130.89 \text{ kPa}$  (26), a Young's modulus of elasticity in circumferential and thickness direction of  $74.07 \text{ kPa}$  (27), and Poisson's ratio of  $0.45$  (27). The inlet boundary condition of the fluid domain was an airflow waveform, which is produced by mechanical ventilation in intubated patients. The airflow was assumed to be laminar with a constant flow profile. Properties of air were assumed to be those at  $25 \text{ }^\circ\text{C}$ . A pressure accounting for the impedance pressure for the rest of the airways was applied at the outlet of the fluid domain (28). A no-slip boundary condition was applied at the fluid-solid interface. A zero-displacement boundary condition was applied to the solid domain at the inlet and outlet to represent a tethering of the airway wall from other tissues and organs (29).

## 2.6 Methods of analysis

A transient analysis with a time step of  $0.01 \text{ sec}$  was performed to study airflow velocity, airway pressure, WSS, airway displacement, and airway stress. WSS is the tangential stress at the airway walls due to fluid viscosity and is related to a transverse velocity gradient (30). Stress distributions in the airway walls were analyzed by employing the von Mises stress, which is associated with distorting the shape of material (31). To eliminate the effect of initial conditions, the simulations were performed for three inhaling/exhaling cycles.

The effects of maximum flow rate during mechanical ventilation on airflow velocity, airway

pressure, WSS, airway displacement, and airway stress in the bifurcation were studied by implementing two flow rate waveforms:  $30$  and  $60 \text{ l/min}$  in the trachea. Input flow waveforms from mechanical ventilation at the trachea are shown in Fig. 3. To obtain the flow rate at airway generation 3, the continuity equation was applied between the trachea and airway generation 3. The obtained flow rate was then applied as the inlet boundary condition of the fluid domain. The flow waveforms were constructed by assuming that the tidal volume was  $700 \text{ cm}^3$ . The passive exhalation was described by the following equation.

$$v(t) = -\frac{V_0}{\tau} e^{-t/\tau}$$

where  $v$  is airflow velocity ( $\text{m/s}$ ),  $t$  is time ( $\text{s}$ ),  $V_0$  is the tidal volume ( $\text{cm}^3$ ), and  $\tau$  is a time constant equal to the product of lung compliance and resistance. The time constant in this study was chosen such that the ratios between the duration of inhalation and exhalation were  $1/2$  and  $1/4$  for airflow rates of  $30$  and  $60 \text{ l/min}$ , respectively (1).

To investigate the effect of airway wall tissue flexibility on airflow velocity, airway pressure, and WSS in the bifurcation, analyses were carried out assuming the airway walls to be rigid or flexible. For the rigid model, analysis was performed only on the fluid domain. The bifurcation in this case acts like a rigid tube that cannot be deformed by fluid forces from the airflow; therefore, there is no stress on the airway walls. For the flexible model, analysis was performed on both fluid and solid domains. The bifurcation in this case acts like a flexible tube that can be deformed by fluid forces from the airflow. Therefore, stress in the airway walls is considered in this analysis. The FSI algorithm (15) was implemented for the flexible model.

## 3 Results and Discussions

### 3.1 Airflow velocity

Airflow velocity patterns for both flow waveforms at the end of inhalation were similar (see Figure 4). High airflow velocity spread throughout G3.

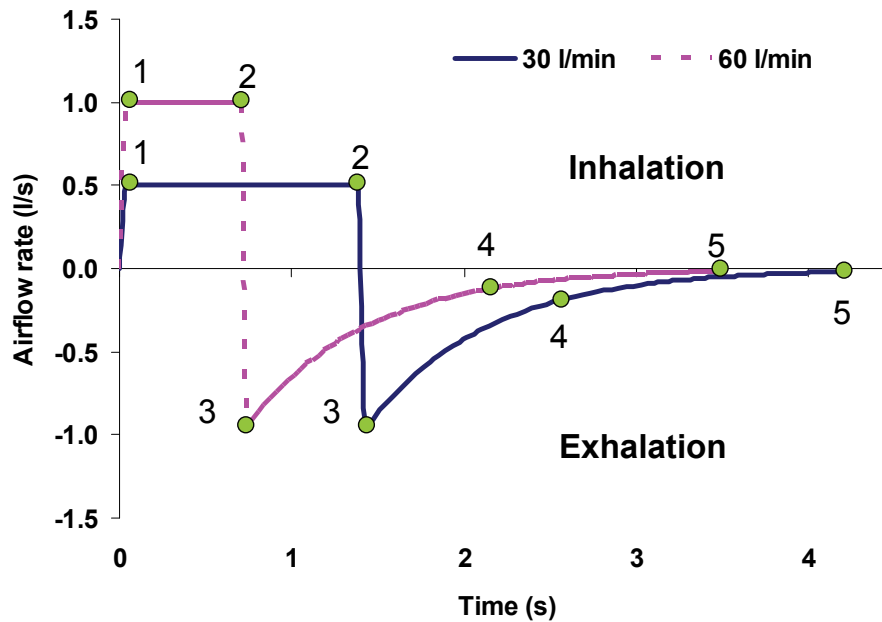


Figure 3: Flow waveforms of active inhalation with a constant flow rate and passive exhalation for airflow rates of 30 and 60 l/min. Five points along the flow waveform that were used to study the tissue flexibility effect are illustrated.

After the first bifurcation, high airflow velocity moved toward medial side of G4. Airflow velocity in both G3 and G4 was symmetric; however velocity profiles in G5 were not symmetric. Airflow velocity in the branch G5M was higher than that in the branch G5L. The difference in airflow velocity in G5 was from high airflow velocity at the medial side of G4. Airflow velocity in all branches increased when the airflow rate increased. The maximum airflow velocity for 30 l/min was 3.247 m/s and this maximum airflow velocity increased approximately 85% when airflow rate increased to 60 l/min.

Patterns of the airflow velocity for the flexible and rigid models were similar at both airflow rates. Airflow velocity from the flexible model was slightly lower than those from the rigid model because of an airway expansion during the inhalation. Table 2 shows the differences in airflow velocity from the flexible and rigid models at each point along the airflow waveform. The maximum differences between both models were at the beginning of the exhalation (point 3) for both airflow rates. They were 15.82% and 61.52% for airflow

rates of 30 and 60 l/min, respectively.

### 3.2 Airway pressure

High pressure areas were at the beginning of G3 and at the bifurcations for both flow waveforms at the end of inhalation (see Figure 5). The pressure at the first bifurcation between G3 and G4 was higher than that at the second bifurcation between G4 and G5. Airway pressure at the bifurcations increased when the airflow rate increased. The maximum airway pressure at the end of inhalation for 30 l/min was 67.86 Pa and this maximum airway pressure increased approximately 40% when the airflow rate increased to 60 l/min. The maximum airway pressure at the first bifurcation was about two times higher than that at the second bifurcation.

Airway pressure distributions for the flexible and rigid models were similar. Airway pressures from the flexible model were lower than those from the rigid model due to the tissue flexibility effect. Table 3 shows the differences in airway pressure for the flexible and rigid models at each point along the airflow waveform. The maximum differences

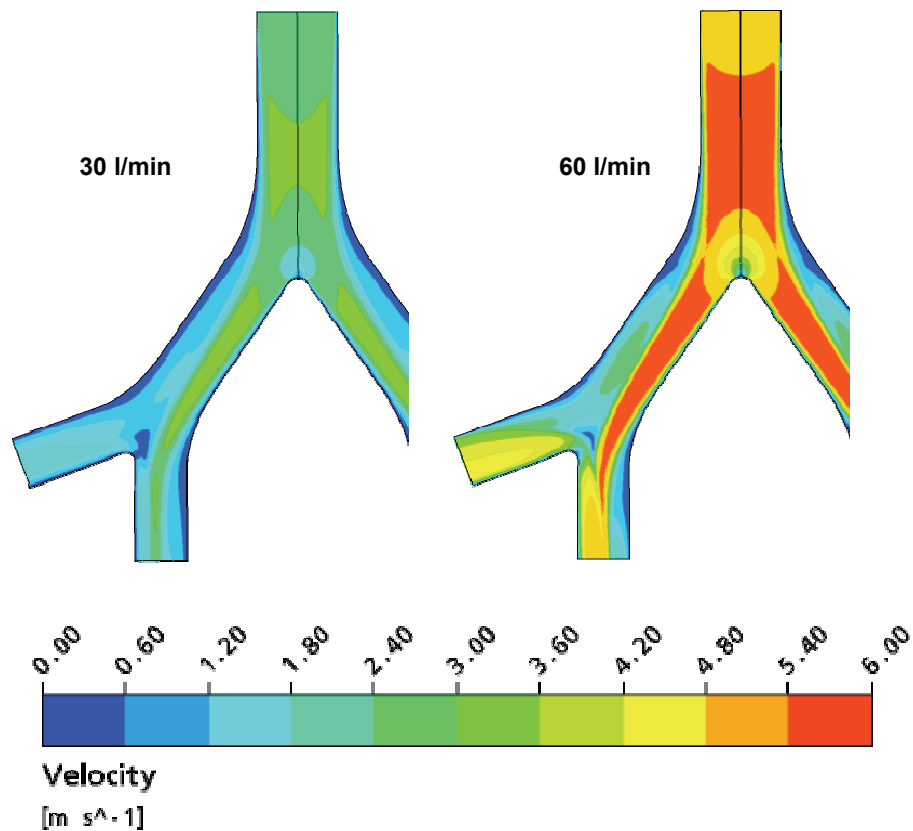


Figure 4: Airflow velocity in airway bifurcation generations 3 to 5 at the end of inhalation (point 2) for airflow rates of 30 and 60 l/min.

Table 2: Comparison of airflow velocity at airflow rate 30 and 60 l/min for the flexible and rigid models

Airflow rates (l/min)	Point	Maximum velocity (m/s)		Error (%)
		Flexible model	Rigid model	
30	1	3.102	3.119	0.55
	2	3.247	3.283	1.11
	3	6.781	7.854	15.82
	4	1.144	1.244	8.74
	5	0.184	0.184	0.00
60	1	5.827	5.858	0.53
	2	5.998	6.115	1.95
	3	6.118	9.882	61.52
	4	1.115	1.168	4.75
	5	0.184	0.184	0.00

between both models were at the beginning of the exhalation (point 3) for both airflow rates. Flexible walls decreased the maximum pressure during mechanical ventilation by 25.06% and 16.91% for 30 and 60 l/min, respectively.

The increase in airway pressure associated with rigid walls suggests that people with stiff airways, e.g., elderly people (32) or asthma patient (33) can experience a higher airway pressure during mechanical ventilation than normal people. High air-

Table 3: Comparison of airway pressure at airflow rate 30 and 60 l/min for the flexible and rigid models

Airflow rates (l/min)	Point	Maximum airway pressure (Pa)		Error (%)
		Flexible model	Rigid model	
30	1	25.022	25.082	0.24
	2	67.863	67.992	0.19
	3	23.374	29.2314	25.06
	4	6.401	6.401	0.00
	5	3.877	3.877	0.00
60	1	53.836	54.142	0.57
	2	95.333	95.764	0.45
	3	23.091	26.995	16.91
	4	6.287	6.287	0.00
	5	3.877	3.877	0.00

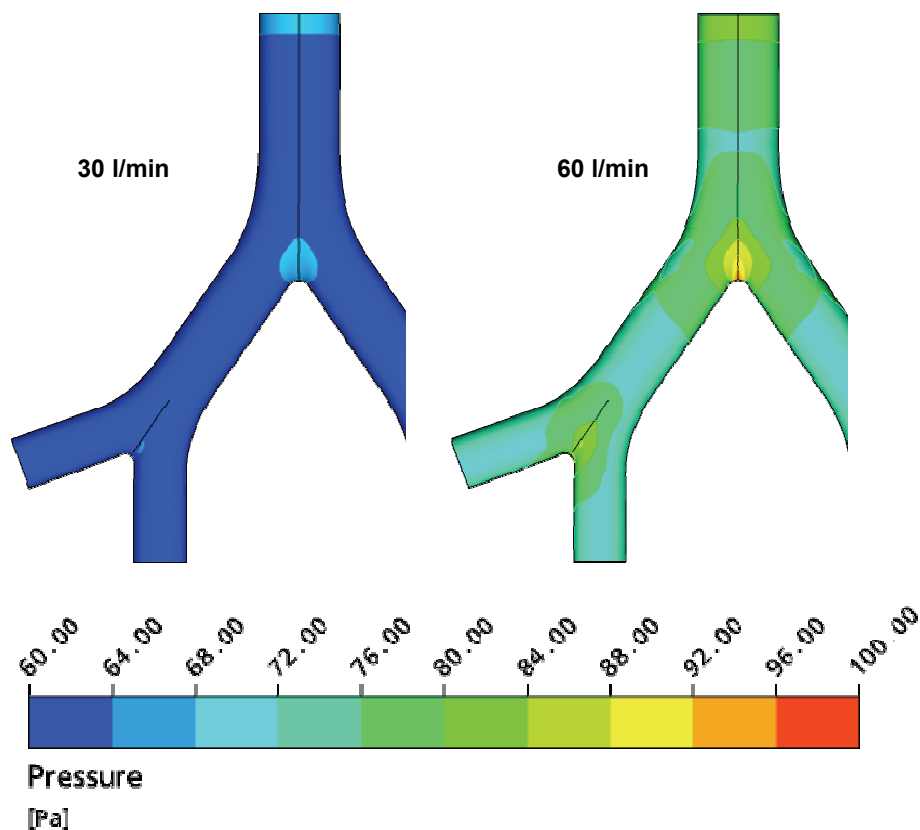


Figure 5: Airway pressure in airway bifurcation generations 3 to 5 at the end of inhalation for airflow rates of 30 and 60 l/min.

way pressure can affect inflammatory mediators (34-36). The overproduction of cytokines can exacerbate lung injury and can lead to an increased mortality of patient with ALI or ARDS. Pressures in the airways can be transmitted throughout the

whole lung via the lung fiber system. If this transmitted pressure is very high, it can cause a mechanical rupture of the lung fiber network especially in diseased regions as may occur with emphysema. This high pressure at the airway walls

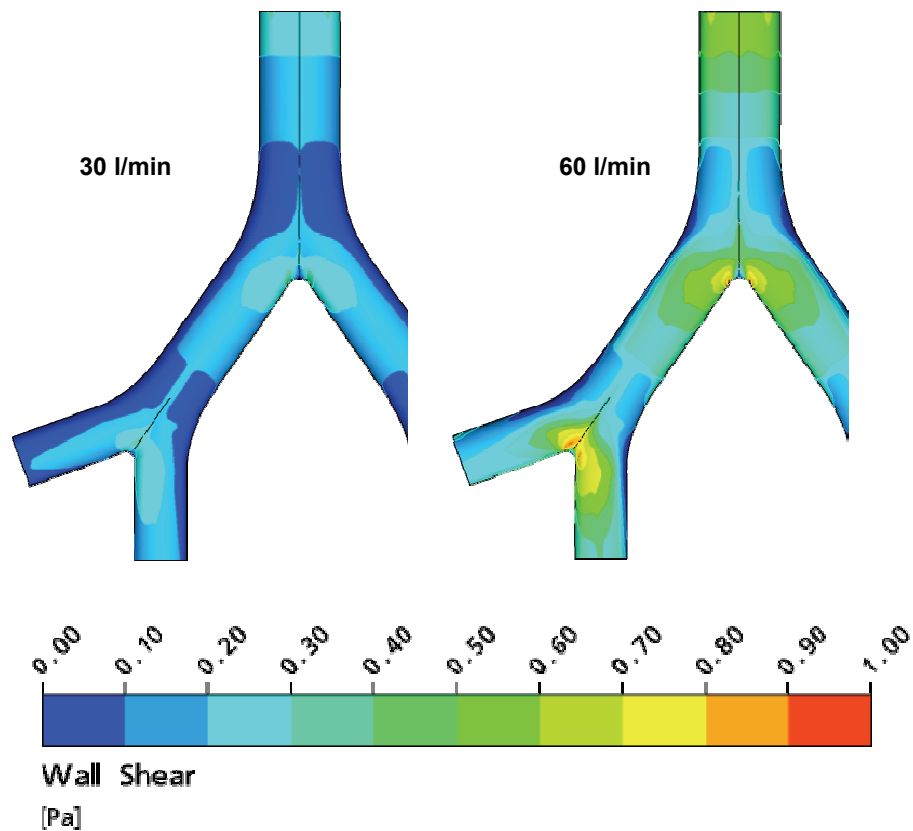


Figure 6: WSS in airway bifurcation generations 3 to 5 at the end of inhalation for airflow rates of 30 and 60 l/min.

also cause a mechanical rupture at alveolar ducts since the axial fibers run from the branching airways to the alveolar structures (37).

### 3.3 Wall shear stress (WSS)

High WSS was observed at the beginning of G3 and at the bifurcations for both flow waveforms at the end of inhalation (see Figure 6). WSS at the medial side of branch G4 was higher than that at the lateral side of branch G4, and WSS in branch G5M was higher than that in branch G5L. WSS increased when the airflow rate increased. The maximum WSS for 30 l/min was 0.421 Pa and this maximum WSS increased approximately 116% when the airflow rate increased to 60 l/min. Distributions of WSS for the flexible and rigid models were similar; however, WSS values from the flexible model were different from the rigid

model. Table 4 shows the differences in WSS for the flexible and rigid models. The maximum differences between both models were at the beginning of the exhalation (point 3) for both airflow rates. The maximum differences in WSS associated with the flexible model during mechanical ventilation were 74.00% and 174.91% for 30 and 60 l/min, respectively. The effects of tissue flexibility on WSS from this study were similar to results from the previous studies in the abdominal aortic aneurysm (AAA) by Leung et al. (38), Torii et al. (39), and Scotti & Finol (40). Their results showed that tissue flexibility can increase or decrease WSS and the influence of WSS highly depended on geometry.

The increases in WSS with the flexible model and with increasing airflow can alter rates of cellular proliferation (41, 42), cell migration (43), cell apoptosis (44), cell turnover (45), cytoskeletal re-

Table 4: Comparison of wall shear stress (WSS) at airflow rate 30 and 60 l/min for the flexible and rigid models

Airflow rates (l/min)	Point	Maximum WSS (Pa)		Error (%)
		Flexible model	Rigid model	
30	1	0.398	0.397	-0.25
	2	0.421	0.417	-0.95
	3	0.677	1.178	74.00
	4	0.061	0.061	0.00
	5	0.007	0.007	0.00
60	1	0.872	0.864	-0.92
	2	0.910	0.884	-2.86
	3	0.558	1.534	174.91
	4	0.059	0.059	0.00
	5	0.007	0.007	0.00

organization (46), nitric oxide (NO) production (47), cell metabolism and gene expression (48) as well as inflammatory mediators (49). When the airflow rate during mechanical ventilation increases, not only does the magnitude of WSS increase but also the frequency of WSS oscillations increases. The increase in frequency of pulsatile airflow can also alter the proliferation rate of a cell (50).

### 3.4 Airway displacements

High airway displacements were observed at the bifurcations for all flow waveforms during the end of inhalation (see Figure 7). The airway displacements at the first bifurcation were lower than those at the second bifurcation. The airway displacements increased when the airflow rate increased. The maximum airway displacement for 30 l/min was 0.2 mm (about 10 % increases in airway diameter) and this maximum airway displacement increased approximately 50% when the airflow rate increased to 60 l/min.

### 3.5 Airway stress

High von Mises stresses were at the bifurcations for all flow waveforms during the end of inhalation (see Figure 8). The von Mises stresses at the first bifurcation were lower than those at the second bifurcation. The von Mises stress increased when the airflow rate increased. The maximum von Mises stress for 30 l/min was 4.8 kPa and

this maximum von Mises stress increased approximately 25% when the airflow rate increased to 60 l/min.

Although the effect of the airflow rate on the airway stress was relatively small compared to changes in the airflow velocity, airway pressure, and WSS, the increase in the airway stress can trigger airway wall remodeling process by increasing the synthesis of Egr-I, fibronectin protein, and the MMP-9/TIMP-1 ratio (51). This increase in Egr-I protein, fibronectin protein, and MMP-9/TIMP-1 ratio from mechanical stress is similar to the response observed in the airway-wall-thickening process of asthma. Stresses in the airway walls can also inhibit airway wall healing process (52).

## 4 Limitations

In this study, the geometry was based on an idealized symmetric model; however, a study by Horsfield et al. (53) showed that airway diameter and branching airways were asymmetric. In addition, material properties of the airway walls in the present study were assumed to be linear with orthotropic properties with similar Poisson's ratio in all direction due to lack of experimental data in the literature. Studies by Ito et al. (54) and Smith et al. (55) showed that the airway wall exhibited viscoelastic properties and nonlinear dynamic behaviors. Further study is needed to investigate the effects of the airway geometry and

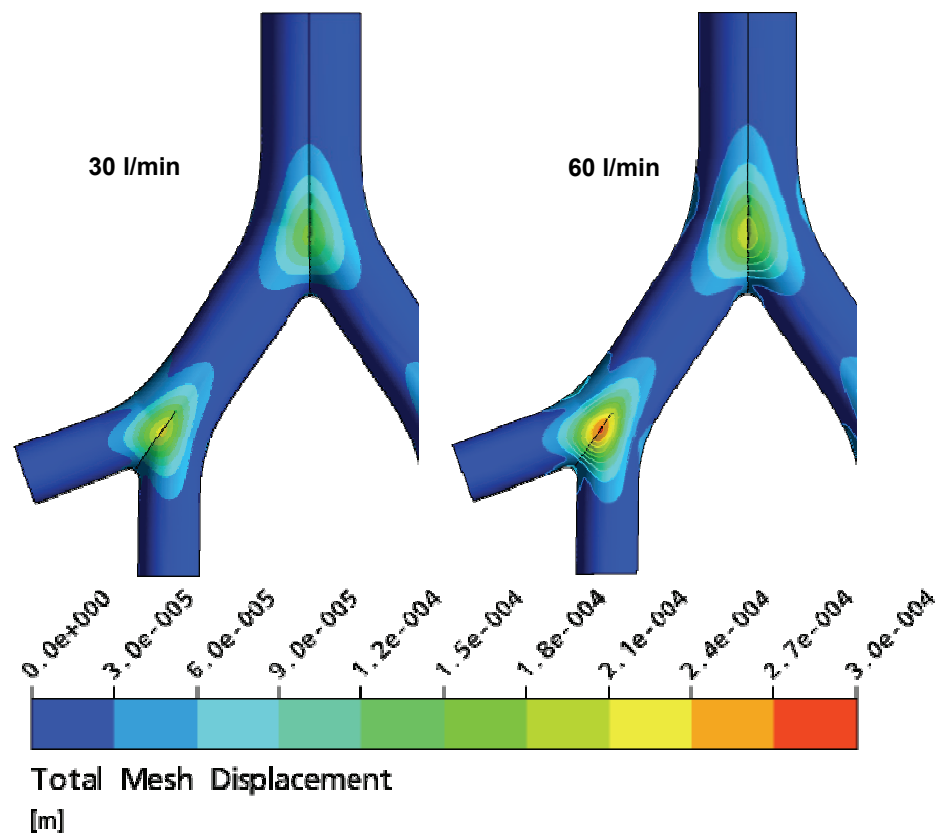


Figure 7: Airway displacement of airway bifurcation generations 3 to 5 at the end of inhalation for airflow rates of 30 and 60 l/min.

airway wall properties on airflow velocity, airway pressure, WSS, and airway stress.

## 5 Conclusion

The airflow velocity, airway pressure, wall shear stress (WSS), and airway stress within the airway generations 3 to 5 were analyzed in this study using the finite element method coupled with the computational fluid dynamics technique. The analysis was performed to investigate the effects of interaction between airflow and airway walls during mechanical ventilation. The simulation results of airflow velocity, airway pressure, WSS, airway displacement, and airway stress were symmetric about airway generation 3 despite the asymmetry at airway generation 5. For the airway generations 3-5 considered in this study, the asymmetric outlets have little influence on the

airflow near the inlet. The results also showed that flexible airway walls decreased airflow velocity and airway pressure as well as altered WSS. Results of this study highlight the importance of including flexible airway walls when analyzing the effects of mechanical ventilation on the airway surface and internal wall structures. Furthermore, this study provides, for the first time, qualitative values of airway pressures, WSS, and airway stress that may be encountered during mechanical ventilation.

## References

1. Lumb, A. B. (2005) *Nunn's Applied Respiratory Physiology* (Butterworth Heinemann, Italy).
2. Imai, Y. & Slutsky, A. S. (2006) in

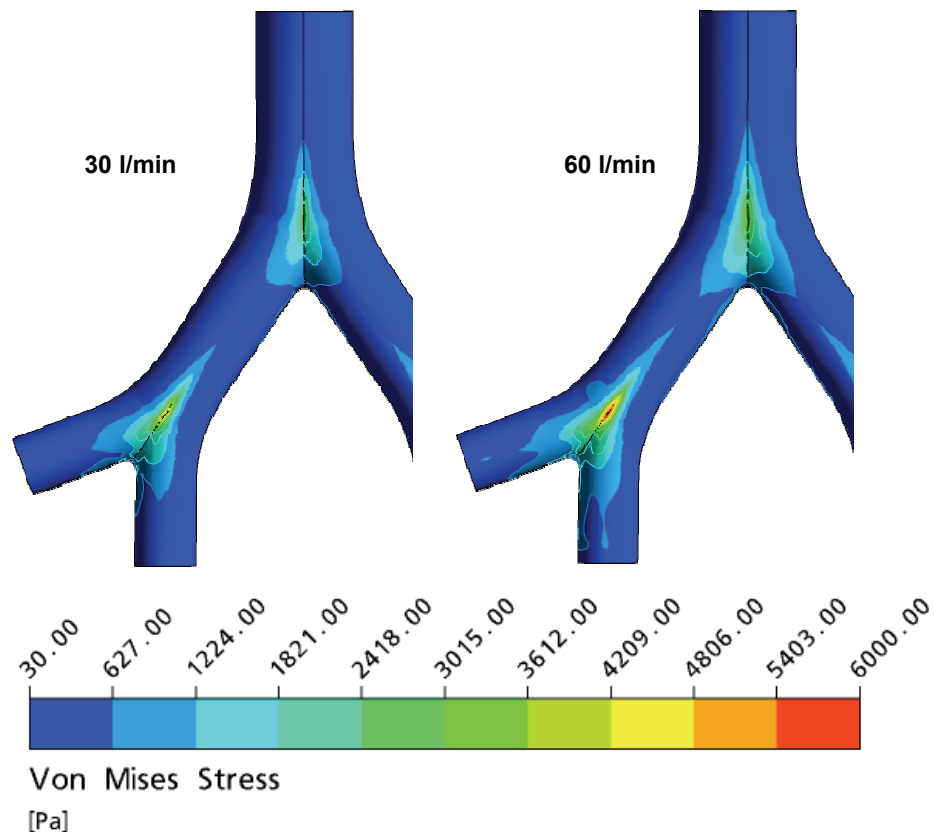


Figure 8: von Mises stress in airway bifurcation generations 3 to 5 at the end of inhalation for airflow rates of 30 and 60 l/min.

- Ventilator-Induced Lung Injury*, eds. Dreyfuss, D., Saumon, G. & Hubmayr, R. D. (Taylor & Francis Group, New York, NY), pp. 267-285.
3. Tobin, M. J. (2001) *The New England Journal of Medicine* **344**, 1986-1996.
  4. Fan, E., Needham, D. M. & Stewart, T. E. (2005) *JAMA* **294**, 2889-2896.
  5. Kleinstreuer, C. & Zhang, Z. (2003) *Journal of Biomechanical Engineering* **125**, 197-206.
  6. Segal, R. A., Guan, X., Shearer, M. & Martonen, T. B. (2000) *Computational and Mathematical Methods in Medicine* **2**, 199-213.
  7. Longest, P. W., Vinchuarkar, S. & Martonen, T. B. (2006) *Journal of Aerosol Science* **37**, 1234-1257.
  8. Brouns, M., Jayaraju, S. T., Lacor, C., Mey, J. D., Noppen, M., Vincken, W. & Verbanck, S. (2007) *Journal of Applied Physiology* **102**, 1178-1184.
  9. Luo, H. Y., Liu, Y. & Yang, X. L. (2007) *Journal of Biomechanics* **40**, 3096-3104.
  10. Yang, X. L., Liu, Y. & Luo, H. Y. (2006) *Journal of Biomechanics* **39**, 2743-2751.
  11. Martonen, T. B., Yang, Y. & Xue, Z. Q. (1994) *Aerosol Science and Technology* **21**, 119-136.
  12. Zhang, Y. & Finlay, W. H. (2005) *Aerosol Science and Technology* **39**, 394-399.
  13. Longest, P. W. & Kleinstreuer, C. (2005)

- Aerosol Science and Technology* **39**, 124-138.
14. Reddy, J. N. (1993) *An Introduction to the Finite Element Method* (McGraw-Hill, New York, NY).
  15. ANSYS (2005) *ANSYS 10.0 User Guide* (ANSYS Inc., Canonsburg, PA).
  16. Hlastala, M. P. & Berger, A. J. (2001) *Physiology of Respiration* (Oxford University Press, New York, NY).
  17. ICRP (1994) *Human Respiratory Tract Model for Radiological Protection* (Elsevier Science Ltd., New York, NY).
  18. Habib, R. H., Chalker, R. B., Suki, B. & Jackson, A. C. (1994) *Journal of Applied Physiology* **77**, 441-451.
  19. Horsfield, K. & Cumming, G. (1967) *Bull Math Biophys* **29**, 245-259.
  20. Heistracher, T. & Hofmann, W. (1995) *Journal of Aerosol Science* **26**, 497-509.
  21. Longest, P. W. & Vinchuarkar, S. (2007) *Journal of Biomechanics* **40**, 305-316.
  22. Longest, P. W. & Vinchurkar, S. (2007b) *Medical Engineering and Physics* **29**, 350-366.
  23. Vinchurkar, S. & Longest, P. W. (2008) *Computers and Fluids* **37**, 317-331.
  24. Zhao, Y. & Lieber, B. B. (1994) *Journal of Biomechanical Engineering* **116**, 488-496.
  25. Sera, T., Satoh, S., Horinouchi, H., Kobayashi, K. & Tanishita, K. (2003) *Journal of Biomechanical Engineering* **125**, 461-471.
  26. Croteau, J. R. & Cook, C. D. (1961) *Journal of Applied Physiology* **16**, 170-172.
  27. Prakash, U. B. S. & Hyatt, R. E. (1978) *Journal of Applied Physiology* **45**, 45-50.
  28. Vassiliou, M. P., Petri, L., Amygdalou, A., Patrani, M., Psarakis, C., Nikolaki, D., Georgiadis, G. & Behrakis, P. K. (2000) *Intensive Care Medicine* **26**, 1057-1064.
  29. Plopper, C. G., Nishio, S. J. & Schelegle, E. S. (2003) *American Journal of Respiratory and Critical Care Medicine* **167**, 2-3.
  30. Shaughnessy, E. J., Katz, I. M. & Schaffer, J. P. (2005) *Introduction to Fluid Mechanics* (Oxford University Press, New York, NY).
  31. Dowling, N. E. (1998) *Mechanical Behavior of Materials* (Prentice Hall, Upper Saddle River, NJ).
  32. Rains, J. K., Bert, J. L., Roberts, C. R. & Paré, P. D. (1992) *Journal of Applied Physiology* **72**, 219-225.
  33. Fredberg, J. J., Jones, K. A., Nathan, M., Raboudi, S., Prakash, Y. S., Shore, S. A., Butler, J. P. & Sieck, G. C. (1996) *Journal of Applied Physiology* **81**, 2703-2712.
  34. Dhanireddy, S., Altemeier, W. A., Matute-Bello, G., O'Mahony, D. S., Glenny, R. W., Martin, T. R. & Liles, W. C. (2006) *Laboratory Investigation* **86**, 790-799.
  35. Goldstein, I., Bughalo, M. T., Marquette, C. H., Lenaour, G., Lu, Q. & Rouby, J. J. (2001) *American Journal of Respiratory and Critical Care Medicine* **163**, 958-964.
  36. Ranieri, V. M., Suter, P. M., Tortorella, C., Tullio, R. D., Dayer, J. M., Brienza, A., Bruno, F. & Slutsky, A. S. (1999) *JAMA* **281**, 54-61.
  37. Gattinoni, L., Carlesso, E., Cadringer, P., Valenza, F., Vagginelli, F. & Chiumello, D. (2003) *European Respiratory Journal* **47** (suppl.), 15S-25S.
  38. Leung, J. H., Wright, A. R., Cheshire, N., Crane, J., Thom, S. A., Hughes, A. D. & Xu, Y. (2006) *BioMedical Engineering Online* **5**, doi:10.1186/1475-925X-5-33.

39. Torii, R., Oshima, M., Kobayashi, T., Takagi, K. & Tezduyar, T. E. (2007) *Computers and Fluids* **36**, 160-168.
40. Scotti, C. M. & Finol, E. A. (2007) *Computers and Structures* **85**, 1097-1113.
41. Kadohama, T., Nishimura, K., Hoshino, Y., Sasajima, T. & Sumpio, B. E. (2007) *Journal of Cellular Physiology* **212**, 244-251.
42. Stiebellehner, L., Belknap, J. K., Ensley, B., Tucker, A., Orton, E. C., Reeves, J. T. & Stenmark, K. R. (1998) *Am J Physiol Lung Cell Mol Physiol* **275**, L593-L600.
43. Sakamoto, N., Ohashi, T. & Sato, M. (2006) *Annals of Biomedical Engineering* **34**, 408-415.
44. Zeng, Y., Qiao, Y., Zhang, Y., Liu, X., Wang, Y. & Hu, J. (2005) *Cell Biology International* **29**, 932-935.
45. Davies, P. F., Remuzzi, A., Gordon, E. J., Dewey, C. F. & Gimbrone, M. A. (1986) *PNAS* **83**, 2114-2117.
46. Birukov, K. G., Birukova, A. A., Dudek, S. M., Verin, A. D., Crow, M. T., Zhan, X., DePaola, N. & Garcia, J. G. N. (2002) *American Journal of Respiratory Cell And Molecular Biology* **26**, 453-464.
47. Li, Y., Zheng, J., Bird, I. M. & Magness, R. R. (2003) *Biology of Reproduction* **69**, 1053-1059.
48. Papadaki, M. & Eskin, S. G. (1997) *Biotechnology Progress* **13**, 209-221.
49. Yamawaki, H., Pan, S., Lee, R. T. & Berk, B. C. (2005) *Journal of Clinical Investigation*, doi:10.1172/JCI200523001.
50. Balcells, M., Suarez, M. F., Vazquez, M. & Edelman, E. R. (2005) *Journal of Cellular Physiology* **204**, 329-335.
51. Swartz, M. A., Tschumperlin, D. J., Kamm, R. D. & Drazen, J. M. (2001) *PNAS* **98**, 6180-6185.
52. Savla, U. & Waters, C. M. (1998) *Am J Physiol Lung Cell Mol Physiol* **274**, L883-L892.
53. Horsfield, K., Dart, G., Olson, D. E., Filley, G. F. & Cumming, G. (1971) *Journal of Applied Physiology* **31**, 207-217.
54. Ito, S., Majumdar, A., Kume, H., Shimokata, K., Naruse, K., Lutchen, K. R., Stamenovic, D. & Suki, B. (2006) *Am J Physiol Lung Cell Mol Physiol* **290**, L1227-L1237.
55. Smith, B. A., Tolloczko, B., Martin, J. G. & Grutter, P. (2005) *Biophysical Journal* **88**, 2994-3007.